Diagnosis of the Source and Evolution of Medium-Range Forecast Errors for Extratropical Cyclone Joachim

WILLIAM S. LAMBERSON,[a] RYAN D. TORN, AND LANCE F. BOSART

Department of Atmospheric and Environmental Sciences, University at Albany, State University of New York, Albany, New York

LINUS MAGNUSSON

European Centre for Medium-Range Weather Forecasts, Reading, United Kingdom

(Manuscript received 6 February 2016, in final form 11 May 2016)

ABSTRACT

Medium-range forecasts for Cyclone Joachim, an extratropical cyclone that impacted western Europe on 16 December 2011, consistently predicted a high-impact intense cyclone; however, these forecasts failed to verify. The potential source and propagation of forecast errors for this case are diagnosed from the 51-member European Centre for Medium-Range Forecasts Ensemble Prediction System initialized 5 days prior to the cyclone's landfall. Ensemble members are subdivided into two groups: one that contained the eight members that had the most accurate forecast of Joachim and, the other, the eight members that predicted the most intense cyclone. Composite differences between these two subgroups indicate that the difference between these forecasts originate in tropopause-based subsynoptic waves along a deep trough in the eastern Pacific. These errors move eastward over a northern stream ridge centered on the west coast of North America and modulate the evolution of a trough that dives equatorward out of Canada and is associated with the development of Joachim. Forecast error calculations and relaxation experiments indicate that reducing forecast errors associated with these subsynoptic features leads to more accurate forecasts. These results present further evidence that subsynoptic errors, especially those originating in the warm sector of a cyclone, can be a significant source of downstream forecast errors.

1. Introduction

The last 30 years have been characterized by a significant improvement in the quality of medium-range (3–10 day) forecasts of midlatitude weather systems. Presently, 6-day forecasts issued by the European Centre for Medium-Range Weather Forecasts (ECMWF) for the Northern Hemisphere extratropics are as accurate as 5-day forecasts issued in the early 2000s, 4-day forecasts issued in the mid-1990s, and 3-day forecasts issued in the early 1980s (Richardson et al. 2013). These forecast accuracy gains are generally attributed to more sophisticated data assimilation methods [e.g., better incorporation of satellite data and the development of the four-dimensional variational data assimilation (4DVAR) scheme] and more sophisticated model formulations (e.g., higher vertical resolution, higher horizontal resolution, and better physics parameterizations).

Despite significant improvements to the average predictability of midlatitude weather systems, short- to medium-range forecasts of individual high-impact extratropical cyclones are still occasionally characterized by large errors. Examples from North America include the snowstorm of 26–27 December 2010, which was poorly predicted 3–5 days in advance (Zheng et al. 2013), and the ''surprise'' snowstorm of 24–25 January 2000, which was poorly forecasted even 1 to 2 days in advance (Zhang et al. 2002). Examples from Europe include Cyclones Martin and Lothar from December 1999, both of which were poorly predicted 1–3 days in advance (Leutbecher et al. 2002). While losses from tropical cyclones are often larger and receive more

[a] Current affiliation: I. M. Systems Group, Inc., Rockville, Maryland.

Corresponding author address: William S. Lamberson, NOAA/NWS/NCEP/IMSG/Weather Prediction Center, 5830 University Research Ct., College Park, MD 20740.
E-mail: bill.lamberson@noaa.gov

DOI: 10.1175/WAF-D-16-0026.1

attention (Enz et al. 2009; Blake et al. 2007), strong extratropical cyclones can also exact a large human and financial toll. In fact, extratropical cyclones accounted for over 10% of the total insured losses from the top 40 global natural and man-made catastrophes that occurred between 1970 and 2008, with Extratropical Cyclones Lothar and Martin, in particular, combining to account for 10.1 billion U.S. dollars (indexed to 2008) in insured losses and 165 fatalities (Enz et al. 2009). Considering the financial and human toll of severe extratropical cyclones, it is important to provide the best forecasts for these events.

Previous studies have suggested that midlatitude forecast errors for these storms can originate both remotely and in situ. Szunyogh et al. (2000) first noted that midlatitude analysis differences (akin to forecast differences) tend to propagate along the midlatitude waveguide [i.e., potential vorticity (PV) gradient] in a manner similar to Rossby wave packets. Langland et al. (2002) provided further support for this hypothesis in their study of forecast errors in the "surprise" snowstorm of 24–25 January 2000. In that case, short-range forecast errors in the intensity and location of the cyclone originated from analysis errors over the eastern Pacific Ocean, and propagated downstream along the waveguide through the forecast. Moreover, they also found that these forecast errors tended to exhibit downstream development characteristics (e.g., Simmons and Hoskins 1979; Chang and Orlanski 1993; Orlanski and Sheldon 1995; Hakim 2003) that allowed the errors to propagate faster than individual synoptic-scale troughs and ridges. Expanding upon this work, Hakim (2005) found that, on average, forecast errors maximize at the tropopause and propagate at the group velocity. This result makes intuitive sense because disturbances located at the tropopause are associated with the organized vertical motions that induce surface cyclones and anticyclones in the midlatitudes. This result is also consistent with the idealized results of Tribbia and Baumhefner (2004), who showed that midlatitude predictability is impacted through baroclinic instability.

The idea that forecast errors for extratropical cyclones originate well upstream and propagate downstream in a manner similar to Rossby wave packets has been substantiated by more recent work. Zheng et al. (2013) and Chang et al. (2013) showed that differences between ensemble forecasts of an extratropical cyclone's track and intensity can originate well upstream as forecast differences between the ensemble members. These forecast differences (akin to forecast errors) then propagate downstream in coherent packets to ultimately impact the forecasted track and intensity of the cyclone. In addition, Majumdar et al. (2010) found that the location where additional observations would have maximum forecast error reduction in medium-range forecasts of high-impact winter weather over North America tended to be located near Japan 4–7 days prior.

Errors in medium-range forecasts of midlatitude weather systems can originate from a multitude of sources. Investigating the impact of analysis differences (akin to forecast errors) on forecasts, Swanson and Roebber (2008) found that the magnitude of the 500-hPa analysis difference averaged over the North Pacific Ocean has a statistically significant impact on forecast skill over the continental United States well into the medium range (4–8-day forecasts). One potential source of medium-range forecast errors in the midlatitudes is the warm conveyor belt (WCB) that exists on the eastern side of extratropical cyclones, which transports relatively warm and moist air poleward and upward. The latent heat release, and transport of lower-PV air from the lower to the upper troposphere that occurs with this motion, serves to amplify the ridge downstream of the extratropical cyclone (Wernli 1997; Joos and Wernli 2012; Chagnon et al. 2013). Numerous theoretical studies have shown that the evolution of the flow downstream from the WCB (i.e., the flow's predictability) is highly sensitive to the evolution of the WCB (Schemm et al. 2013; Riemer and Jones 2010). Observational studies have confirmed that WCBs have a large impact on the evolution of the downstream flow. In particular, Davies and Didone (2013), as well as Dirren et al. (2003), found that wrongly predicted WCBs can significantly alter Rossby waves propagating along the waveguide and thus, can radically alter the evolution of the flow downstream from the WCB. As a consequence, accurate downstream forecasts may require having a good forecast of the WCB region (e.g., Grams et al. 2011; Torn 2010).

A recent example of an extratropical cyclone that exhibited a lack of predictive skill in the medium range was Cyclone Joachim, which impacted northwestern Europe during December 2011. Cyclone Joachim attained a maximum intensity of 964 hPa while bringing high winds of over 150 $km\,h^{-1}$ to northwestern Europe (AIR Worldwide 2011). Despite knocking out power to an estimated 300 000 households in France, forecasts issued prior to 13 December 2011 consistently predicted that Cyclone Joachim would attain a maximum intensity of 940 hPa and have a much larger impact on northwestern Europe. By contrast, forecasts issued on and after 13 December 2011 were characterized by a more accurate forecast of a weaker Cyclone Joachim. This suggests that uncertainty in some process or feature was significantly reduced during the 12–13 December 2011 time period. This study seeks to understand what caused

TABLE 1. Summary of features associated with the development of Joachim.

Abbrev	Description
C1	Bering Sea cyclone
R1	Highly amplified ridge downstream from C1
C2	Cyclone that develops along the trailing cold front of C1
R2	Short-wave ridge that develops downstream from C2
PVS	Potential vorticity streamer located between R1 and R2
TN	Northern stream trough that develops as R2, PVS, and R1 break off a piece of the polar vortex
TS	Southern stream trough
C3	Cyclone produced through the interaction of TS with a baroclinic zone

medium-range forecasts of Cyclone Joachim to be highly inaccurate and why there was a rapid increase in forecast accuracy for Joachim between forecasts issued on 12 December and those issued on 13 December.

The remainder of this paper proceeds as follows. Section 2 provides an overview of the event, including its poor medium-range forecasts. Section 3 describes the dataset and methodology used in this study, while section 4 explores the dynamical processes responsible for the poor medium-range forecasts. A summary and conclusions are given in section 5.

2. Overview of Cyclone Joachim

a. Synoptic evolution of the event

Prior to evaluating sources of error in forecasts for Cyclone Joachim, an overview of the atmosphere's evolution prior to and during the event is presented. The focus of this summary is on the relevant synoptic- and subsynoptic-scale features in the atmosphere prior to and during the development of Joachim that will play a role in the accuracy of forecasts for Joachim. For clarity, a list of these relevant features is presented in Table 1.

The ECMWF analysis at 0000 UTC 11 December (Fig. 1a) shows a mature, vertically stacked surface cyclone with a minimum central pressure of 958 hPa located over the Bering Sea (hereafter C1) and a highly amplified ridge (hereafter R1) downstream, with a narrow corridor of strong southerly flow. Along the trailing cold front of C1 (denoted by a pronounced pressure trough equatorward and east of C1), a second surface cyclone with a minimum central pressure of 992 hPa (hereafter C2) is located near 42°N, 172°W. Downstream of C2, a short-wave ridge (hereafter R2) is beginning to amplify. The amplification of R2 is accompanied by the creation of a PV streamer (hereafter PVS) between ridges R1 and R2. At this time, C2, R2, and PVS are all subsynoptic-scale features embedded in a larger, planetary-scale trough.

Over the next 24 h, the flow over western North America splits into distinct northern and southern streams. In the northern stream, C2 rapidly deepens into a mature extratropical cyclone with a minimum central pressure of 966 hPa as it moves to 57°N, 153°W by 0000 UTC 12 December (Fig. 1b). The strengthening of C2 is associated with the amplification of R2 over Alaska. At the same time, both PVS and R1 have thinned while moving poleward and eastward. As the northern stream wave train composed of R2, PVS, and R1 moves poleward and eastward, it begins to interact with the reservoir of high PV (denoted by tropopause potential temperature values below 300 K) poleward of 75°N, forcing a piece of it to break off. This feature, labeled TN, is associated with a potent trough in the northern stream and will be shown to be the most important feature in the development of Joachim. Concurrently, the remnants of a PV streamer deposited by an anticyclonic wave breaking event that occurred 2 days earlier (not shown) is evident as a weak trough (local minimum in the 2-PVU tropopause potential temperature field; $1\ \text{PVU} = 10^{-6}\ \text{K kg}^{-1}\ \text{m}^2\ \text{s}^{-1}$) over the southern United States (hereafter TS).

The surface analysis at 0000 UTC 13 December (Fig. 1c) indicates that R2 has progressed eastward and started to break anticyclonically. As this occurs, PVS and R1 continue to move eastward and thin, while TN moves eastward and equatorward to ~60°N, 80°W. TS moves to a position over the eastern United States, near a low-level baroclinic zone located at ~35°N, 65°W.

Continuing with the analysis of the atmosphere prior to the development of Cyclone Joachim, Fig. 1d shows that by 0000 UTC 14 December, R2 has completely merged with PVS and R1. In addition, R2 and TN move farther east as R2 continues to break anticyclonically. At the same time, TS has moved off the coast of the southeastern United States and has interacted with the baroclinic zone there to produce a 1004-hPa surface cyclone (hereafter C3). Over the next 24 h (Fig. 1e), interaction between TS and C3 allows the central pressure of C3 to drop to 992 hPa as it moves to ~40°N, 50°W by 0000 UTC 15 December (Fig. 1e), while TN moves farther east to ~55°N, 30°W by 0000 UTC 15 December. As a consequence, TN is located ~2000 km northeast of C3 and will not have the opportunity to phase with C3. By contrast, forecasts initialized 4 to 5 days prior to 0000 UTC 15 December predicted C3 and Cyclone Joachim to be the same system. In reality, Joachim develops 12 h later along the warm front east of C3 that is denoted by a pronounced pressure trough that extends northeast from C3 (Fig. 1e). At 0000 UTC 16 December 2011

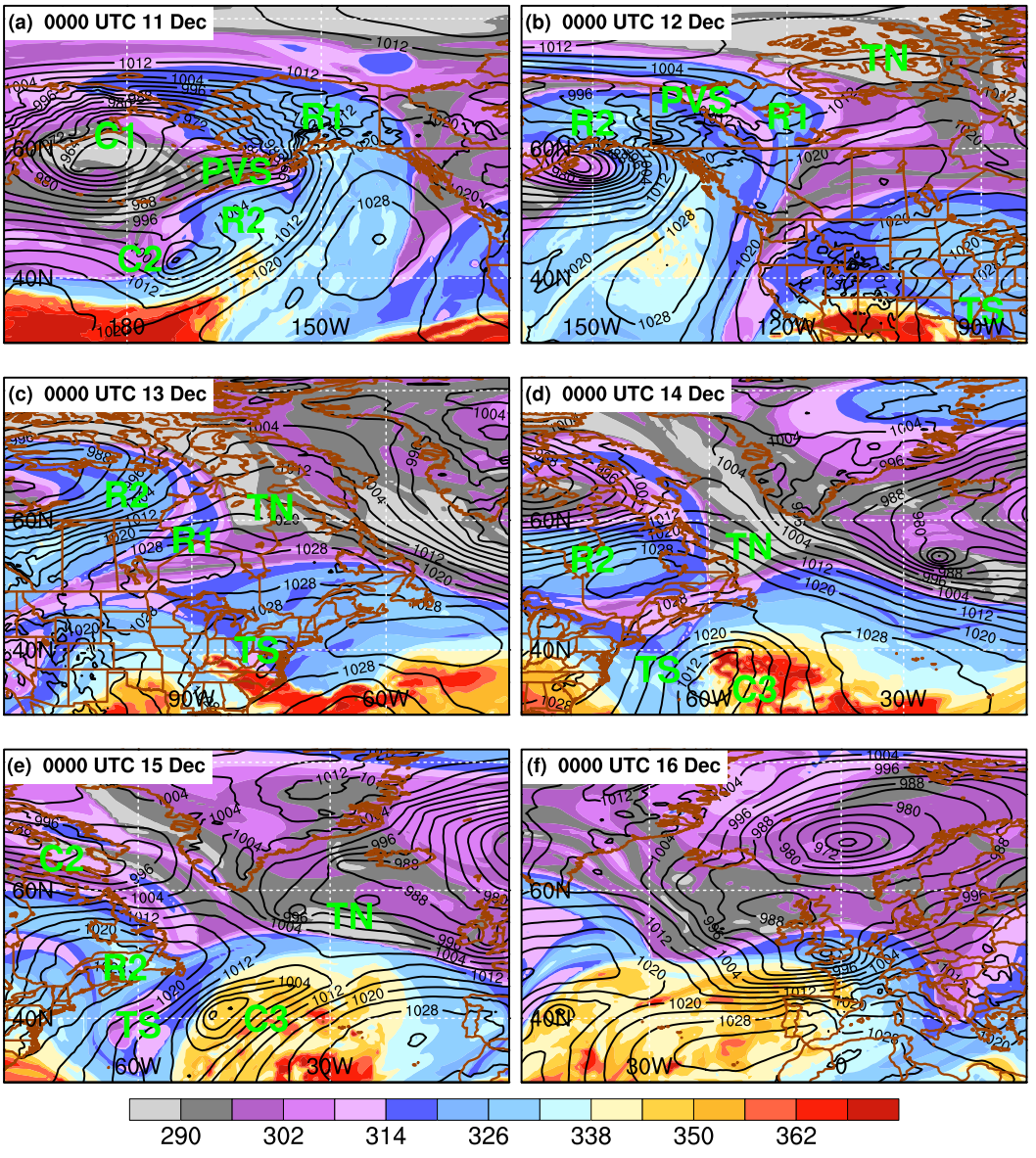

FIG. 1. Analyses of potential temperature on the 2-PVU surface (shaded; K) and sea level pressure (black contours, every 4 hPa) from the deterministic ECMWF. Analyses are valid at (a) 0000 UTC 11 Dec, (b) 0000 UTC 12 Dec, (c) 0000 UTC 13 Dec, (d) 0000 UTC 14 Dec, (e) 0000 UTC 15 Dec, and (f) 0000 UTC 16 Dec 2011. Features identified in the text are labeled in green.

(Fig. 1f), Joachim is a 978-hPa surface cyclone over the southern United Kingdom, while the remnants of C3 are still located over the Atlantic at ~40°N, 45°W. Over the next 12 h, Joachim deepens to its maximum intensity of 964 hPa as it moves to a position over northern Germany by 1200 UTC 16 December (not shown).

b. *Deterministic and ensemble forecasts*

Medium-range (4–8 day) forecasts for Cyclone Joachim from several global models were relatively inaccurate. To illustrate this, 6- and 5-day forecasts verifying at 0000 UTC 16 December 2011 from the deterministic ECWMF and the deterministic GFS are shown in Figs. 2a–d, with the ECMWF analysis valid at 0000 UTC 16 December 2011 (Fig. 2e) included for comparison. The 6- and 5-day deterministic forecasts from the ECMWF depict a cyclone that is approximately 30 hPa deeper than, and 500 km to the north of, its analyzed intensity and position. In addition, medium-range forecasts from the ECMWF overpredict the

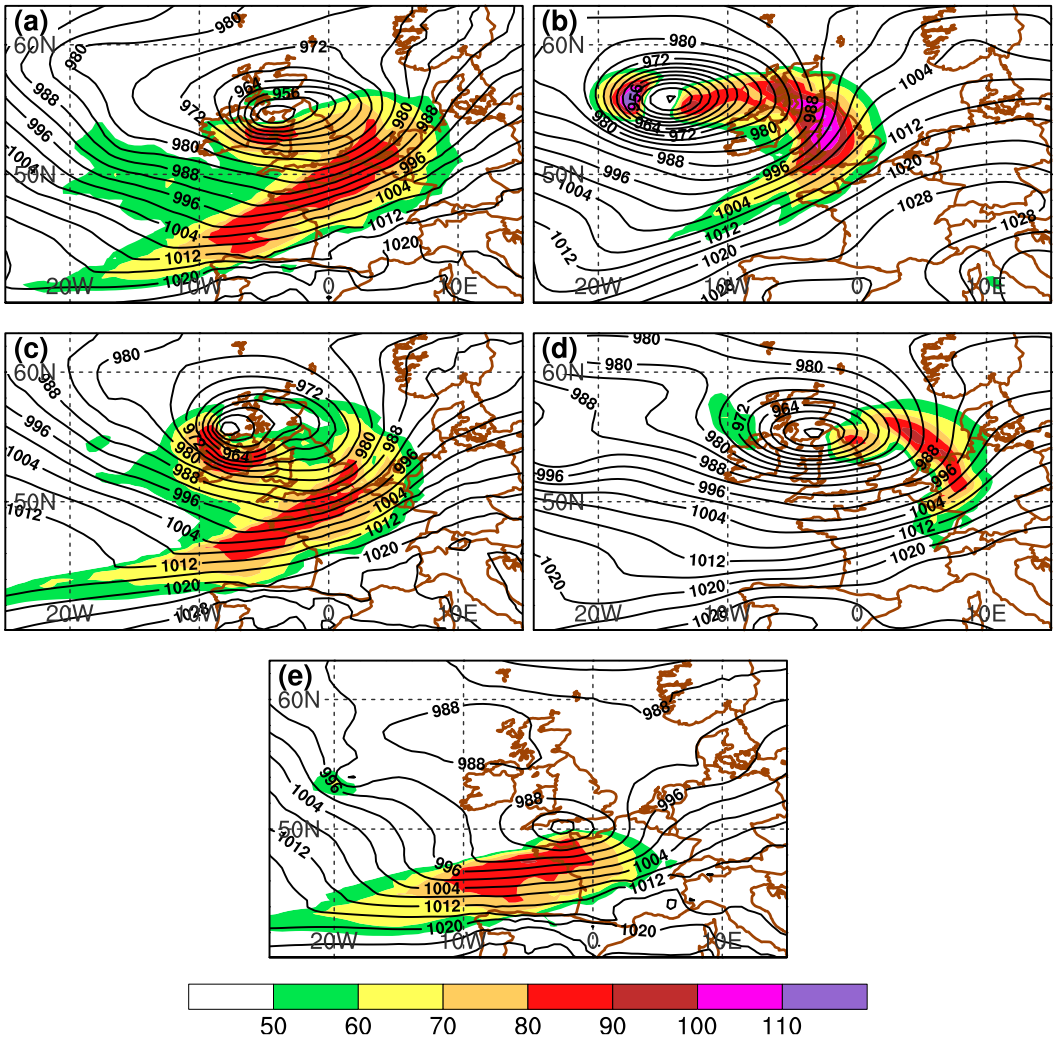

FIG. 2. Deterministic forecasts valid at 0000 UTC 16 Dec 2011 for 850-hPa wind speed (shaded, kt; 1 kt = 0.51 m s^{-1}) and sea level pressure (black contours, every 4 hPa) from (a) ECMWF initialized at 0000 UTC 10 Dec, (b) GFS initialized at 0000 UTC 10 Dec, (c) ECMWF initialized at 0000 UTC 11 Dec, and (d) GFS initialized at 0000 UTC 11 Dec. (e) The ECMWF analysis valid at 0000 UTC 16 Dec.

strength and areal extent of high winds associated with the cyclone. The GFS forecasts for Joachim were of similarly poor quality, and also had intensity errors of approximately 30 hPa and location errors of 500 km.

In addition to the overintensification issues in deterministic GFS and ECMWF forecasts, most members of the ECMWF ensemble had similar position and intensity errors. Figure 3 shows the evolution of the cyclone position and intensity forecasts valid at 0000 UTC 16 December as a function of initialization time for the ECMWF Ensemble Prediction System (ENS). The 6- and 5-day forecasts (Figs. 3a,b) consistently overpredict the strength of the cyclone as ~30 of the 51-members predict a cyclone with a minimum pressure < 950 hPa, which corresponds to a minimum sea level pressure error ≥ 15 hPa, while the ensemble-mean position is ~500 km northwest of the actual storm. By the 4-day forecast (Fig. 3c), the envelope of possible position and intensity forecasts begins to shift toward the observed values as the number of extreme (<940 hPa) members markedly decreases. The 3-day forecast (Fig. 3d) brings a complete shift of the envelope of solutions as both the extreme (<940 hPa) and the northerly solutions are no longer members of the ensemble. As the event draws nearer, the 2- and 1-day forecasts further hone in on the correct solution (Figs. 3e,f), as both the forecasted intensity and position of Joachim collapse toward their observed values. The rapid shift in the envelope of ensemble forecasts of Joachim's evolution in forecasts initialized between 11 and 13 December suggests that the

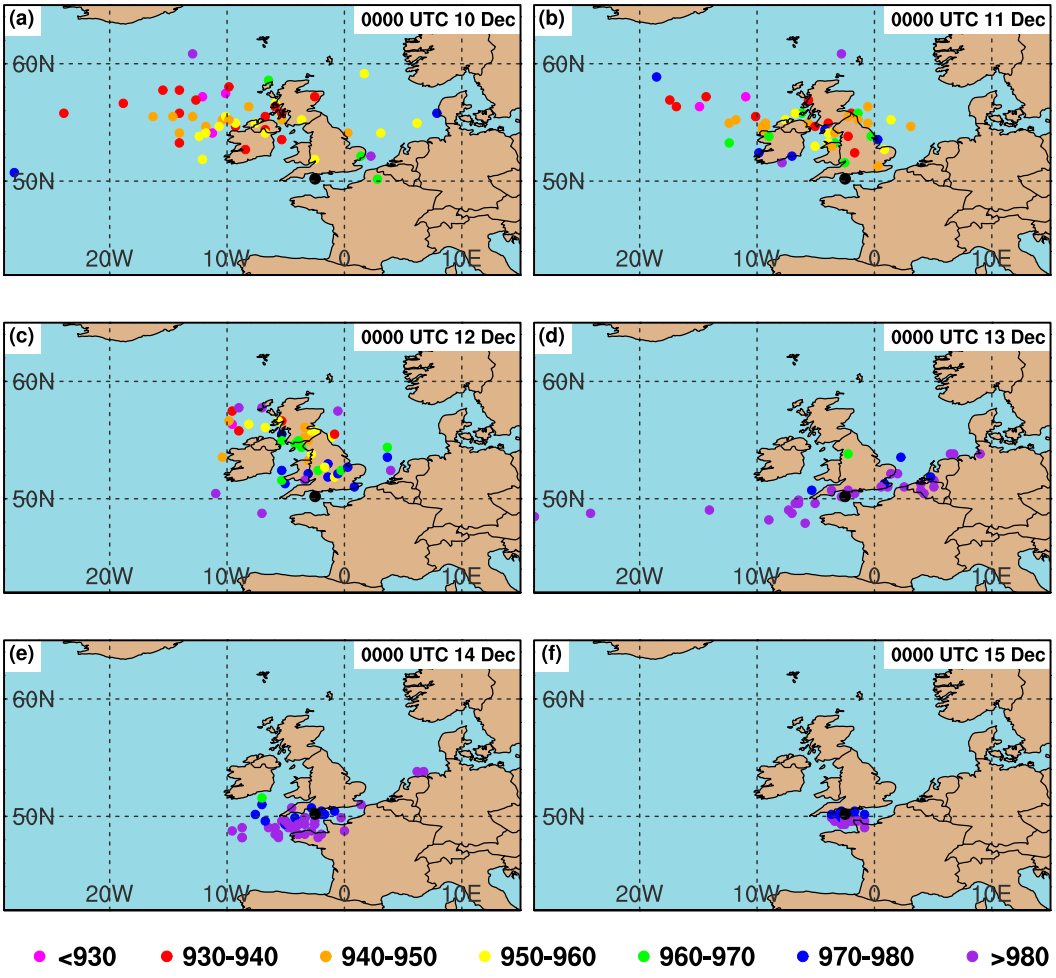

FIG. 3. Location of Joachim's sea level pressure minimum among the 51 members of the ECMWF ENS valid at 0000 UTC 16 Dec and initialized at (a) 0000 UTC 10 Dec, (b) 0000 UTC 11 Dec, (c) 0000 UTC 12 Dec, (d) 0000 UTC 13 Dec, (e) 0000 UTC 14 Dec, and (f) 0000 UTC 15 Dec 2011. The color of each dot represents the strength of Joachim (hPa), according to the legend at the bottom. The black dot shows the location of Joachim's analyzed sea level pressure minimum at 0000 UTC 16 Dec.

uncertainty in some process or feature was significantly reduced during this time period; this study seeks to identify it.

3. Data and methodology

To diagnose the evolution and sources of error in medium-range forecasts for Joachim, medium-range ECMWF ENS (Buizza et al. 2007) forecasts for the event are analyzed. These forecasts are obtained from The Observing System Research and Predictability Experiment (THORPEX) Interactive Global Grand Ensemble (TIGGE) archive (Bougeault et al. 2010). The ECMWF ENS is chosen for this study because it has a larger number of members (51) than any other operational ensemble prediction system, which provides a larger sample of forecasts to analyze and apply statistical analysis methods, and for its well-documented, superior performance over the other operational ensemble prediction systems (e.g., Park et al. 2008). The focus of this study is the forecast initialized at 0000 UTC 11 December, though a similar procedure was carried out on forecasts initialized 24 h before and after 0000 UTC 11 December.

To diagnose the source of errors, the ensemble members are divided into two subgroups based on their forecasts of Joachim. One subgroup contains the members that forecasted the strongest Cyclone Joachim, and hence had the largest intensity errors (hereafter Strong members), while the other subgroup contains the members with the most accurate forecasts of Cyclone Joachim (hereafter Accurate members). The Strong

TABLE 2. Accurate members for the 0000 UTC 11 Dec 2011 initialization of the ECMWF EPS.

Member	Track error rank	Intensity error rank	Summed intensity and track error rank
18	1	9	10
9	15	1	16
25	10	6	16
8	6	11	17
28	7	10	17
48	2	16	18
5	5	15	20
26	17	3	20

subgroup is composed of the eight members that contain the strongest cyclone (measured by minimum sea level pressure) between 0000 UTC 15 December and 1200 UTC 17 December. By contrast, the Accurate subset is composed of the eight members that had the lowest track and intensity errors, with respect to the ECMWF analysis for Joachim. More specifically, each member's track and intensity errors are first computed with respect to the location and magnitude of Joachim's minimum in sea level pressure in ECMWF analyses every 12 h between 1200 UTC 15 December and 0000 UTC 17 December. Track and intensity errors are then averaged over time and independently ranked from 1 to 51, with 1 corresponding to the member with the lowest average error of the 51 members. Finally, the track and intensity error ranks are added together and the eight members with the lowest combined intensity and track error ranks are selected as the Accurate members. This methodology for selecting the Accurate members effectively equates track and intensity errors even though they have different units. The Accurate members for the 0000 UTC 11 December initialization of the ECMWF ENS are listed in Table 2 with their attendant track and intensity error ranks.

The ensemble mean forecasts of Joachim's minimum sea level pressure for the two subgroups are shown in Fig. 4a, while Fig. 4b shows Joachim's forecasted track between 1200 UTC 15 December and 0000 UTC 17 December from all 51 ensemble members. The Strong subgroup ensemble mean (red line in Fig. 4a) clearly shows that the Strong members lie at the lower end of the minimum sea level pressure distribution. In addition to being too strong, Joachim undergoes cyclogenesis in the Strong members over the central Atlantic as early as 0000 UTC 14 December. Moreover, the strong members (red lines) are mainly on the northern side of the track distribution (Fig. 4b). Selection of the Strong members did not involve track error, so this result alone suggests that the strength and position of Joachim are not independent. The Accurate subgroup ensemble mean (blue line in Fig. 4a) forecasted that Joachim would attain a peak intensity of 962 hPa at 0600 UTC 16 December. This intensity is much closer to Joachim's actual peak intensity of 966 hPa, but it occurs ~6 h too early. In addition, the cyclogenesis time and location are within 12 h and 200 km of the analysis values for each member of the Accurate subgroup. As expected, Fig. 4b shows that the Accurate members (blue lines) have a more southerly and accurate track of Joachim than the rest of the ensemble members.

The dynamical processes responsible for the differences between the two subgroups are diagnosed by comparing the mean of the Accurate members against the mean of the Strong members for various atmospheric quantities as a function of lead time. As in Torn et al. (2015), this analysis employs normalized differences (i.e., standardized anomalies), which are defined as

$$\Delta x_i = \frac{\overline{\mathbf{x}}_i^{\text{Accurate}} - \overline{\mathbf{x}}_i^{\text{Strong}}}{\sigma_{x_i}}, \tag{1}$$

where $\overline{\mathbf{x}}_i^{\text{Accurate}}$ ($\overline{\mathbf{x}}_i^{\text{Strong}}$) denotes the mean of the ith state variable for the Accurate (Strong) ensemble members, and σ_{x_i} is the ensemble standard deviation of $\mathbf{x}_i$ computed from all members. Normalizing the difference between the two subsets has the benefit of permitting comparison among different vertical levels, fields, and times. In addition, normalizing aids in the interpretation of differences on a single vertical level because it downplays the differences along large gradients, which can have large absolute differences as a result of displacement errors.

The statistical significance of the subset differences was assessed using a bootstrap resampling without replacement (Livezey and Chen 1983). Specifically, two subsets of ensemble members, equal in size to the Strong and Accurate subgroups, were randomly selected from the 51-member ensemble. Then, the difference between the ensemble mean of the two, randomly chosen subsets was calculated. This process was repeated 1000 times to obtain the 95% confidence bounds on the subgroup differences. The benefit of this particular method is that the statistical significance can be evaluated without assuming a Gaussian distribution for $\mathbf{x}_i$.

4. Diagnosis of forecast error sources and evolution

a. *Subgroup differences*

One hypothesis for the origin of the error in forecasts for Joachim is that errors in upstream features

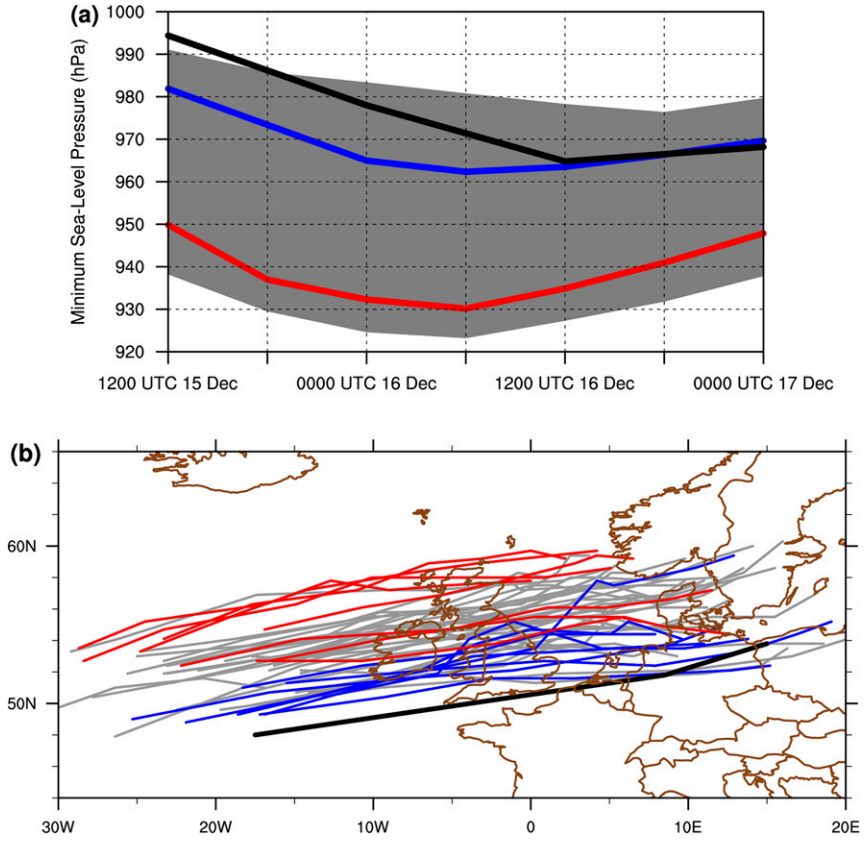

FIG. 4. (a) Ensemble mean minimum sea level pressure of Joachim as a function of time for the Accurate (blue line) and Strong (red line) members of the 0000 UTC 11 Dec 2011 initialization. The black line indicates Joachim's minimum sea level pressure in ECMWF analyses. Gray shading denotes the range of Joachim's minimum sea level pressure among the 51 ensemble members. (b) Ensemble forecasts from the 0000 UTC 11 Dec initialization of the ECMWF ENS of Joachim's track between 1200 UTC 15 Dec and 0000 UTC 17 Dec. Strong member tracks are indicated by red lines, Accurate member tracks are indicated by blue lines, and nonsubgroup member tracks are denoted by gray lines. The black line indicates Joachim's track from ECMWF analyses during this time period.

propagated downstream to impact the location of TN relative to TS. This hypothesis is evaluated by looking at differences in vorticity between the Accurate and Strong subgroups at various vertical levels. Differences in vorticity were evaluated because it can be used to illustrate the location and intensity of the relevant features, can be derived from the limited TIGGE dataset, and allows for an investigation of both the horizontal and vertical structure of forecast differences. Vorticity can be an inherently noisy parameter; therefore, differences in vorticity between two sets of ensemble members may not produce a consistent signal. Instead, vorticity is smoothed by taking an area average of vorticity within 400 km of a given grid point. This effectively reduces the noise in the vorticity field so that a meaningful signal in the subgroup differences can be extracted. Several radii were investigated, but a 400-km radius was chosen because it yielded the most consistent signal over time (not shown).

Figure 5 shows the evolution of subgroup differences in 300-hPa vorticity. At 0 h (Fig. 5a), there is a distinct packet of statistically significant forecast differences located at ~47°N, 167°W (in the vicinity of R2), with a maximum normalized magnitude of 1.6 standard deviations (equivalent to $2.0 \times 10^{-5}\,s^{-1}$). The negative differences to the southwest of, and positive differences to the north of, R2's ensemble mean position indicate that the Accurate members have stronger upper-tropospheric ridging to the southwest of R2 and weaker upper-tropospheric ridging to the north of R2 than the Strong members. Taking a vertical cross section through R2 and its differences at this time shows that forecast differences between the two subgroups are maximized around 300 hPa (i.e., near the tropopause) but

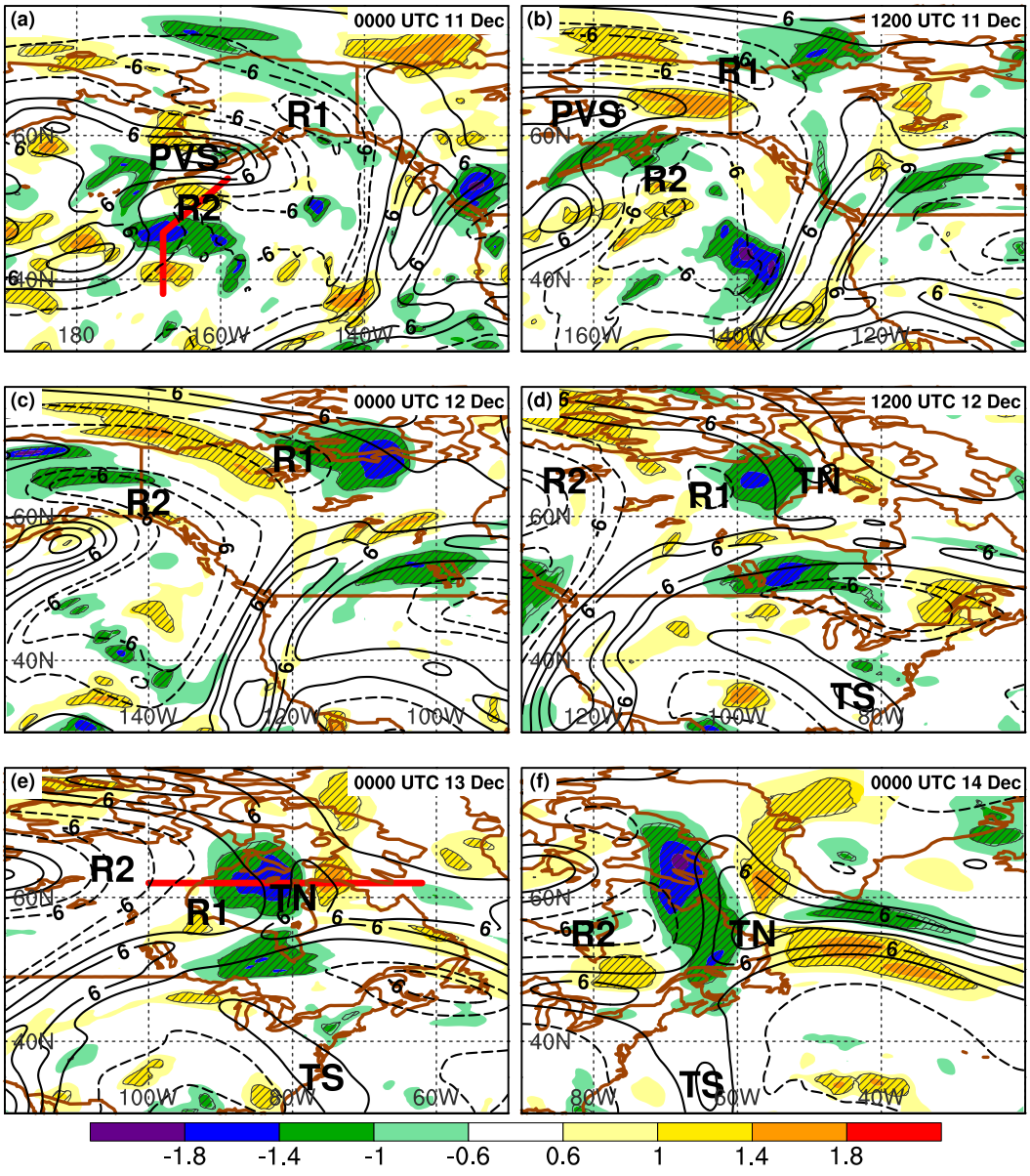

FIG. 5. Normalized difference in 300-hPa vorticity, averaged within 400 km of each point, between the Accurate and Strong members (shading; units: standardized anomaly) at (a) 0, (b) 12, (c) 24, (d) 36, (e) 48, and (f) 72 h for the ECMWF forecast initialized at 0000 UTC 11 Dec 2011. Hatching indicates where the differences between the two subsets are statistically significant at the 95% confidence level. Contours denote the ensemble-mean 300-hPa vorticity within 400 km (10^{-5} s^{-1}). Features identified in the text are labeled in black. Red lines denote cross sections shown in Fig. 6.

are statistically significant between 700 and 200 hPa (Fig. 6a). This cross section confirms that at 0 h, the primary difference between the two subgroups is their analyzed intensity and the locations of R2 and PVS, and that these differences are confined to the mid- to upper troposphere. Taken together, Figs. 5 and 6 show that subgroup differences for the case of Joachim are organized in wave-packet-like structures that maximize on the tropopause, which is consistent with the forecast error structure presented in Hakim (2005).

Over the next 12 h, the packet of subgroup differences associated with R2 move poleward along a waveguide (here, a waveguide is defined as an area with a large gradient in PV) so that the area of negative differences that were located to the southwest of R2 at 0 h is now aligned with R2's axis in the ensemble mean (Fig. 5b).

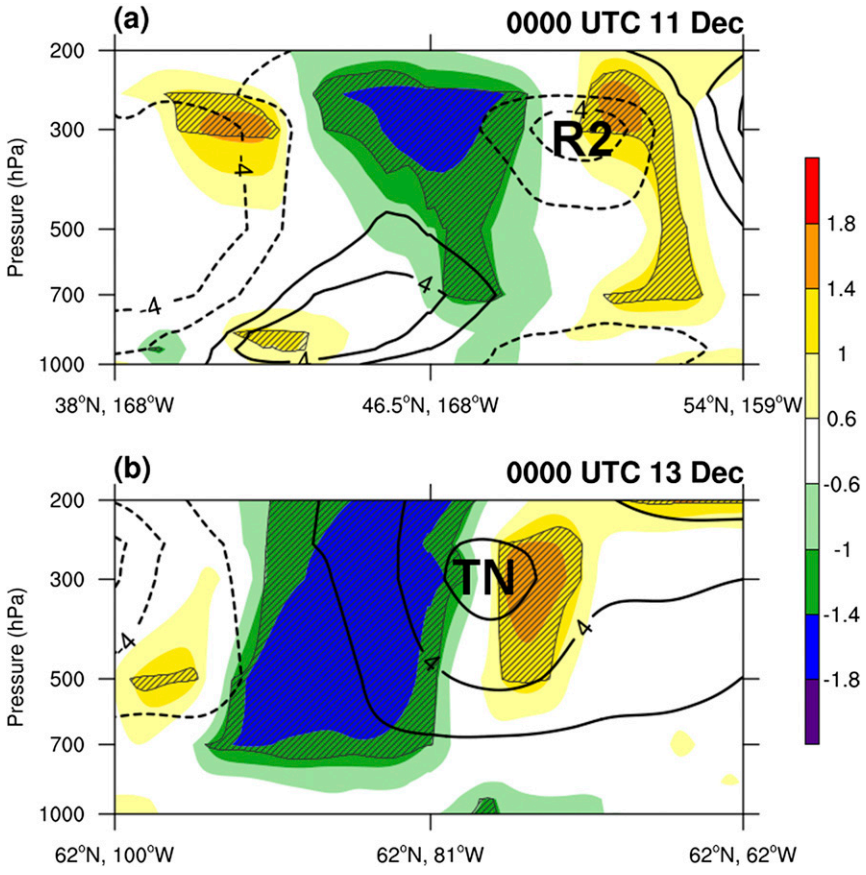

FIG. 6. Cross sections of normalized difference in vorticity between the Accurate and Strong members (shading; units: standardized anomaly) at (a) 0 and (b) 24 h. Hatched regions indicate where the difference is statistically significant at the 95% confidence level. Contours denote the ensemble-mean vorticity within 400 km ($10^{-5}\,s^{-1}$). Features identified in the text are labeled in black.

The area of positive differences located just poleward of R2 at 0 h is now located along and poleward of PVS's axis. This indicates that the Accurate members have a more intense R2 than the Strong members and a PVS that is elongated and displaced slightly poleward of its position in the Strong members. In addition, an area of negative differences has developed to the east of R1, indicating that R1 extends farther eastward in the Accurate members than in the Strong members.

By 24 h, the coherent packet of differences moves eastward and is now centered on R1 (Fig. 5c). This pattern of differences suggests that the relative accuracy of the forecasts for Joachim depends on the location of R1, with the more accurate members characterized by a more eastward position of R1. Over the next 12 h, R1 and R2 begin to interact with and deform the reservoir of high PV over the pole, eventually breaking off a piece of the high PV to form the northern stream trough, TN. As this occurs, vorticity differences on the order of 0.8 standard deviations ($1.4 \times 10^{-5}\,s^{-1}$) begin to develop to the east of TN (Fig. 5d). Together with the established negative differences to the west of R1, the positive differences east of TN indicate that relatively accurate forecasts of Joachim are characterized by an R1 and a TN that are forecasted to be approximately 100 km farther eastward. By 48 h, the positive differences east of TN increase in normalized magnitude to 1.8 standard deviations ($3.0 \times 10^{-5}\,s^{-1}$) and become statistically significant (Fig. 5e). A cross section taken through the area of the largest differences at this time (Fig. 6b) shows that forecast differences near TN are maximized between 500 and 200 hPa. This indicates that forecast differences in tropopause-based disturbances remain the source of variability in medium-range forecasts of Joachim. Twenty-four hours later, the differences centered on TN have increased in magnitude and indicate that TN is farther east in the Accurate members (Fig. 5f). Figures 5 and 6 show that the vorticity differences tend to propagate downstream, in tandem with the feature they were initially associated with. This contrasts with

other studies that suggest forecast errors tend to exhibit downstream development characteristics that allow them to propagate downstream faster than individual synoptic-scale troughs and ridges (Langland et al. 2002).

While it is possible to trace coherent differences between the Accurate and Strong members in the northern stream, this is not the case for the southern stream. At all lead times, the differences in the southern stream are generally not statistically significant. The lack of forecast differences in the southern stream suggests that variability in the forecasted evolution of the northern stream prior to the development of Joachim is the primary source of variability in the medium-range forecasts for the cyclone. In particular, the subgroup differences indicate that the position of TN ultimately dictates the intensity and track of Joachim, with the position of TN being modulated by R2, PVS, and R1 earlier in the forecast. Among the Accurate members, TN is located too far east to phase with C3, and consequently Joachim develops along the baroclinic zone of C3, similar to what occurs in reality (cf. Fig. 1). Among the Strong members, TN is located farther west, which allows it to merge with TS as C3 develops in the western Atlantic. This merger leads C3 to develop into an intense extratropical cyclone while crossing the Atlantic Ocean toward western Europe.

Forecasts initialized 24 h before and after exhibit a similar sensitivity to the location of TN. To briefly illustrate this, Fig. 7 shows subgroup differences between the Accurate and Strong subgroups at 0000 UTC 14 December for four initialization times.[1] Similar to the subgroup differences for the 0000 UTC 11 December initialization, the subgroup differences for the other initialization times are concentrated in the northern stream with few, if any, differences around TS in the southern stream. The pattern of differences around TN seen in the other initializations indicates that more accurate forecasts of Joachim are obtained when TN is farther east. Moreover, all four initialization times are characterized by forecast differences that move across the northern stream through Alaska and Canada, though the ultimate source differs from one initialization to another. This result lends even further credence to the idea that the accuracy of medium-range forecasts for Joachim depends heavily on the accuracy of the forecasted evolution of the northern stream.

b. PV inversion

The subgroup analysis indicates that early time forecast differences in R2, PVS, R1, and eventually TN may play a large role in determining the strength and track of Joachim; however, the dynamical explanation is missing. To diagnose the dynamical mechanism by which these errors impact the downstream state, statistical PV inversion (e.g., Hakim and Torn 2008) is employed to derive the upper-tropospheric winds associated with the difference in the 250-hPa PV between the Accurate and Strong members. Using the concepts of PV ''action at a distance'' (e.g., Hoskins et al. 1985), statistical PV inversion can be used to demonstrate how a more amplified R2 seen in the Accurate members early in the forecasts eventually leads to a TN that is located farther eastward. Here, PV inversion on absolute subgroup differences is used to demonstrate how the winds associated with the forecast differences of one feature can modify the other features. This technique involves computing the linear operator that maps from a particular PV field to the wind field using a singular value decomposition of the ensemble forecast fields. A drawback of this method is that results obtained with a small ensemble relative to the number of degrees of freedom can suffer from statistical artifacts. However, a large advantage of statistical PV inversion is that it does not require the specification of boundary conditions. The interested reader is directed to Hakim and Torn (2008) for a more complete description of statistical PV inversion. For brevity, only a few times are discussed here.

Figure 8a shows the inverted winds from the negative PV difference associated with R2 at 18 h. As expected, this negative elliptical PV anomaly has anticyclonic winds associated with it. The perturbation winds on the order of 1 m s^{-1} are directed from the higher values of ensemble-mean PV to the north of the negative PV differences near 65°N, 130°W toward PVS. This would be expected to intensify PVS and help shift it farther to the east. Indeed, Fig. 8b shows that by 30 h, the PV differences associated with PVS (blue contours) indicate that PVS is located eastward of its ensemble mean position among the Accurate members. At this time, perturbation winds associated with the positive PV differences near PVS are cyclonic and southerly to southwesterly. Over R1 (~65°N, 115°W), these winds are 0.5 m s^{-1} and are acting to advect R1 farther eastward relative to its mean position. Finally, inverting the negative PV difference between R1 and TN (around ~65°N, 97°W) at 1200 UTC 12 December (36 h) demonstrates how TN might have ended up farther east. As a reminder, this negative PV difference is indicative of R1's farther east location in the Accurate members compared to the Strong members. The winds associated with this difference in the PV field are

[1] Accurate and Strong subgroups for the other initializations are selected in the same manner as the Accurate and Strong subgroups for the 0000 UTC 11 December 2011 initialization of the ECMWF ENS.

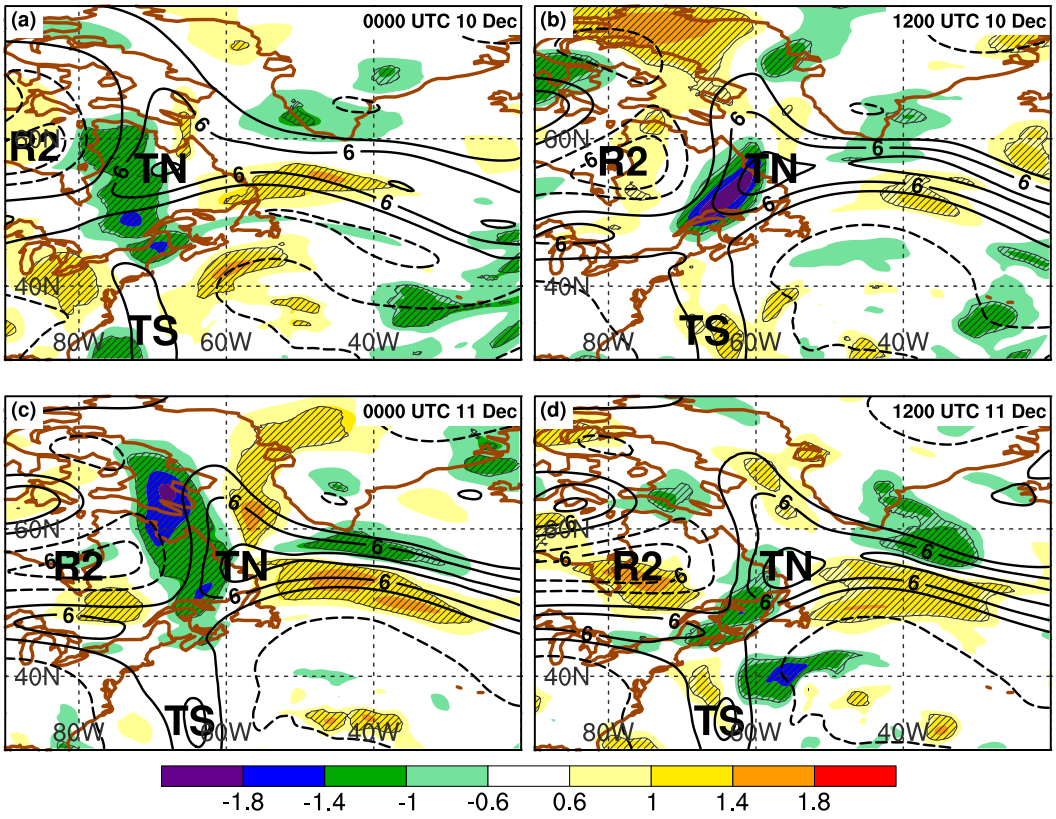

FIG. 7. Normalized difference in 300-hPa vorticity between the Accurate and Strong members (shading; units: standardized anomaly) valid at 0000 UTC 14 Dec 2011 from the ECMWF ENS initialized at (a) 0000 UTC 10 Dec, (b) 1200 UTC 10 Dec, (c) 0000 UTC 11 Dec, and (d) 1200 UTC 11 Dec. Hatching indicates where the differences between the two subsets is statistically significant at the 95% confidence level. Contours denote the ensemble-mean 300-hPa vorticity within 400 km (10^{-5} s^{-1}). Features identified in the text are labeled in black.

northwesterly and roughly 2 m s^{-1} in magnitude over TN (~65°N, 92°W). This indicates that R1's farther eastward position in the Accurate members is imparting a northwesterly wind perturbation on TN that will push it farther southeastward (i.e., farther downstream).

Although the perturbation winds in Fig. 8 are relatively small (0.5–2 m s^{-1}), integrating these winds over time aligns well with the observed position differences in PVS, R1, and TN between the Accurate and Strong members. At 84 h, the observed position difference between TN in the two subgroups is roughly 250 km. In particular, a 250-km position error corresponds with a wind difference of 1.5 m s^{-1}, which is similar to the perturbation winds shown. While small, an ~250-km position difference can have a large impact on the degree of phasing between the two troughs within the flow that is characterized by large-scale deformation. Numerical simulations have shown that phasing between two troughs in background flow that is characterized by deformation is highly sensitive to a narrow range of parameters including the strength of the background deformation as well as the size, location, and strengths of the troughs (e.g., Hakim et al. 1996). Given that TN is located in background flow characterized by deformation, it is quite plausible that the observed differences in TN's location can mean the difference between phasing with C3 and not phasing with C3.

c. *Forecast error*

The subgroup analysis and PV inversion strongly suggest that early time forecast differences in R2, PVS, R1, and eventually TN play a large role in determining the strength and track of Joachim. Thus, it follows that the Accurate members should have more accurate forecasts of R2, PVS, and R1 than the Strong members, which subsequently leads to more accurate forecasts of Joachim. This hypothesis is tested by verifying each member's 300-hPa area-averaged vorticity forecast in the vicinity of R2 and PVS as well as R1 and TN against the corresponding time analysis fields at various lead

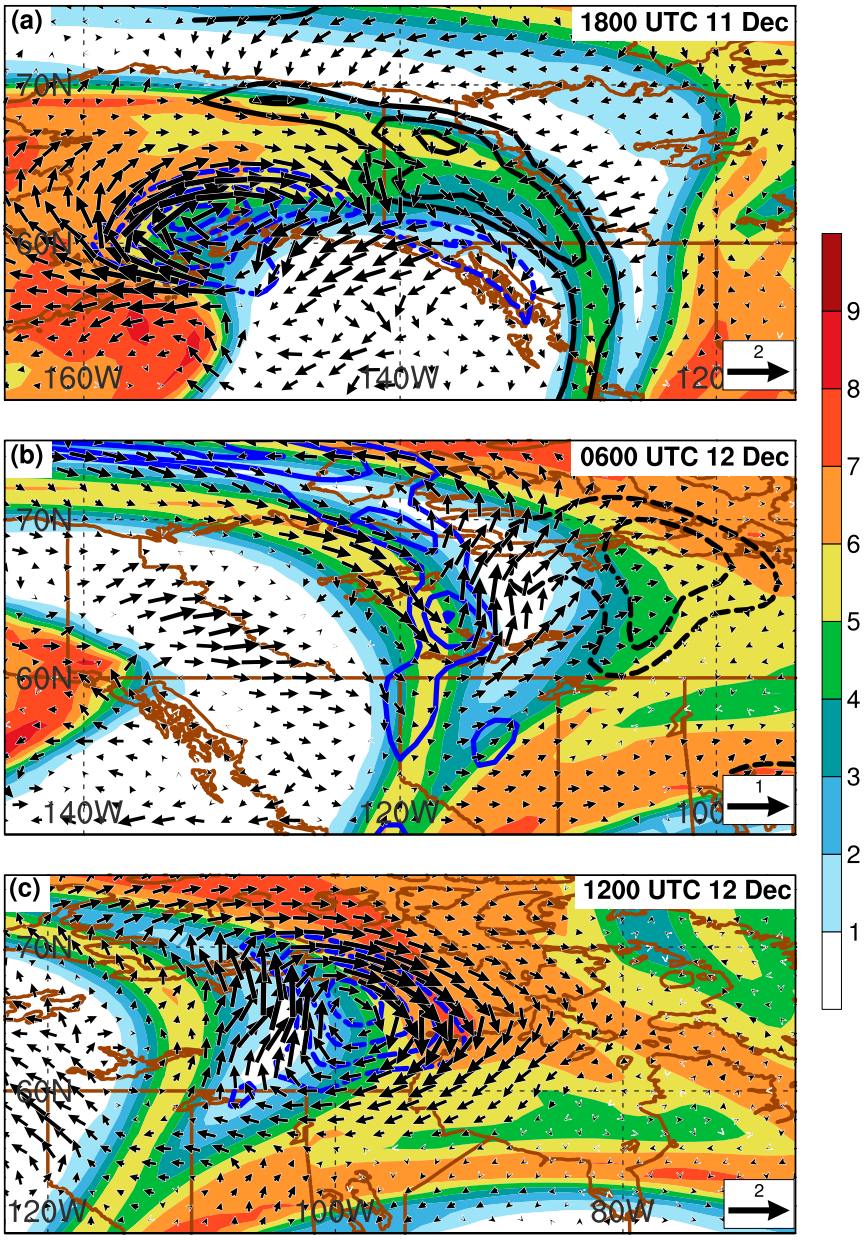

FIG. 8. Statistical piecewise Ertel PV inversion of the of the 250-hPa PV subgroup differences associated with (a) R2 at 18 h, (b) PVS at 30 h, and (c) R1 at 36 h. The blue contours (every 0.3 PVU) denote the area of subgroup PV differences being inverted, while black contours (every 0.3 PVU) denote the differences in 250-hPa PV. Vectors give the inverted 250-hPa wind field ($m\,s^{-1}$), and the ensemble mean 250-hPa PV field is shaded (PVU).

times using pattern correlation. In particular, the pattern correlation is carried out for grid points where the difference between the two subgroups was statistically significant at the 95% level. This was done so that the pattern correlations focused on the areas with the largest differences between the two subgroups. Forecast errors associated with R2 and PVS are evaluated together because forecast differences originate with these two features, while forecast errors associated with R1 and TN are lumped together because the forecast differences associated with these features are indistinguishable by 24 h (Fig. 5c).

Figure 9a shows that by 1200 UTC 11 December (12 h), the Accurate members have more accurate forecasts of R2 and PVS; moreover, the difference in the pattern correlation score is determined to be statistically

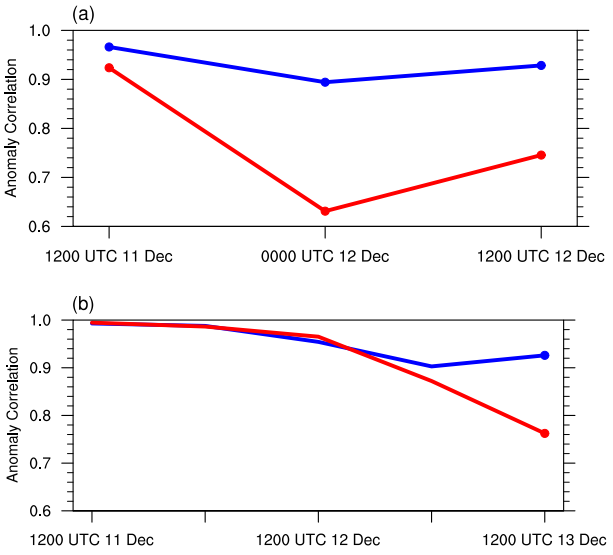

FIG. 9. Pattern correlation of forecasted 300-hPa vorticity within 400 km with the corresponding analysis field in the vicinity of (a) R2 and PVS and (b) R1 and TN. Blue lines show the ensemble mean anomaly correlation for the Accurate members, and red lines show the ensemble mean for the Strong members. Dots indicate times where the difference between the two subgroups is statistically significant at the 95% level.

significant at the 95% level by a *t* test. At 0000 UTC 12 December (24 h), the difference in pattern correlation between the two subsets remains statistically significant, while the difference increases to ~0.40. This result confirms the hypothesis that the Accurate members do have significantly more accurate forecasts of R2 and PVS than the Strong members early in the forecast. Forecast errors for R1 and TN (Fig. 9b) show the same result, but the onset of a statistically significant difference between the two subgroups does not occur until 1200 UTC 13 December (60 h), which corresponds to the time when the forecast differences reach TN. This result further suggests that forecast errors originate with R2 and PVS and then propagate downstream toward TN through the forecast.

d. Relaxation experiments

The previously discussed results suggest that errors in the evolution of the northern stream early in the forecast are responsible for errors in the forecasted intensity and track of Joachim later in the forecast. To further investigate and pinpoint the source of the forecast error for this case, a series of relaxation experiments (e.g., Jung et al. 2010a,b) was conducted. Relaxation is a technique that draws a model forecast toward another value (e.g., that from a reanalysis) during the course of the model's integration. It is generally carried out over a specific area as a means of reducing the forecast error in that area. When compared to the original forecast, the forecast that utilizes relaxation can be used to assess the impact of forecast errors in the relaxation area on the rest of the forecast.

TABLE 3. Summary of ECMWF ENS relaxation experiments.

Acronym	Long description	Relaxation region
CNT	Control	—
NLB	Northern large box	50°–75°N, 40°W–180°
NSB	Northern small box	65°–75°N, 100°W–180°
NMB	Northern minibox	65°–75°N, 120°W–180°
SLB	Southern large box	0°–40°N, 40°W–180°

Here, several relaxation experiments are performed on the 0000 UTC 11 December initialization of the ECMWF ENS, where the forecast is relaxed toward the corresponding control member analysis. The only difference between the relaxation experiments is in the area being relaxed. The four different relaxation areas employed are described in Table 3 and are depicted in Fig. 10a. It is worth noting that forecasts are being drawn toward an analysis that can also have error, which can impact the validity of the results gleaned from comparing forecasts with and without relaxation. For this reason, the relaxation experiments should be viewed as a complement to the other techniques used to identify the source and evolution of Cyclone Joachim's errors.

Relaxation involves adding an extra term of the following form to the prognostic equations of the ECMWF model:

$$-\lambda(\mathbf{x}-\mathbf{x}^{\mathrm{ref}}), \tag{2}$$

where $\mathbf{x}$ is the ensemble state vector and $\mathbf{x}^{\mathrm{ref}}$ is the reference vector toward which the model is drawn (here ECMWF ENS control analysis interpolated in time). In addition, λ controls the strength of the relaxation and has units of $(\text{time step})^{-1}$. For the relaxation experiments employed in this study, $\lambda = 1/3$, indicating that at each time step, the model is corrected using 33.33% of the departure of $\mathbf{x}$ from $\mathbf{x}^{\mathrm{ref}}$ for all variables and levels. The interested reader is directed to Jung et al. (2010a,b) for a more complete description of relaxation.

Previous results suggest that errors in the intensity and position of Joachim originate with several features that move through the northern stream. To assess this, the first relaxation experiment (NLB) uses a large box that captures the evolution of these features during the first 72 h of the forecast. For these ensemble forecasts, Joachim's position and intensity errors are significantly reduced (Fig. 10c). In fact, the forecasts for Joachim produced by relaxation over the NLB area become as

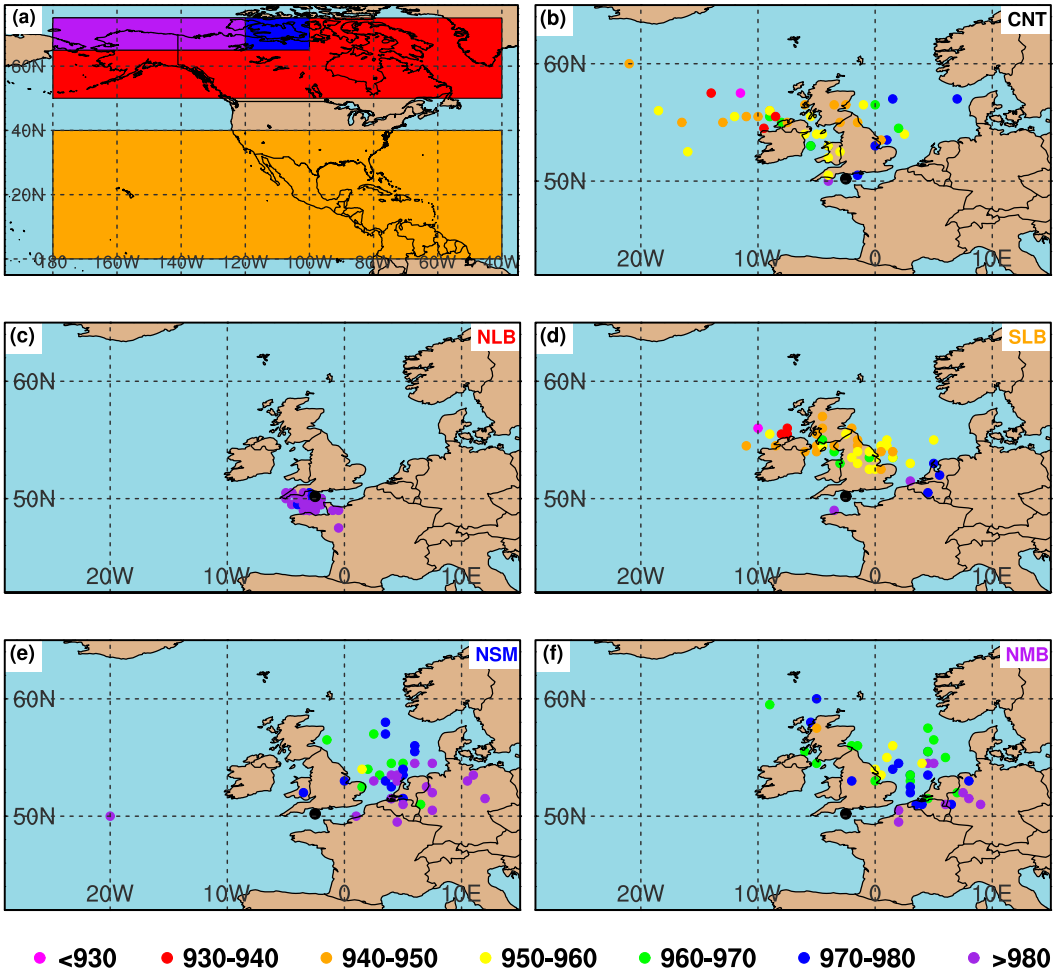

FIG. 10. (a) The four boxes used in the relaxation experiments: purple box, NMB; blue box, NSB; red box, NLB; and orange box, SLB. The results of each experiment are shown by the location of Joachim's sea level pressure minimum among the 51 members of the ECMWF ENS for each relaxation experiment: (b) CNT, (c) NLB, (d) SLB, (e) NSM, and (f) NMB. The color of each dot represents the strength of Joachim (hPa), according to the legend at the bottom of the figure.

accurate as the operational ensemble forecast initialized at 0000 UTC 15 December (cf. Fig. 3f). By contrast, the SLB experiment, where the southern stream is relaxed toward the analysis, still contains ensemble members that are too deep and too far north (Fig. 10d). As a consequence, these results provide further evidence that Joachim's forecast errors originate in and propagate through the northern stream. Finally, two additional relaxation experiments were run with progressively smaller relaxation areas to further pinpoint the error source. Experiments NSB and NMB capture the evolution of R2 and PVS during the first 36 and 24 h of the forecast, respectively. These relaxation experiments (Figs. 10e,f) show an improvement in the forecasted intensity of Joachim as many of the members now forecast Joachim to have a minimum sea level pressure between 970 and 985 hPa. However, experiments NSB and NMB still suffer from large errors in the location of Joachim and, because of this, their forecasts are not nearly as accurate as those obtained during experiment NLB. This could be due to the areas of large forecast errors moving out of the boxes before the relaxation technique has sufficient time to correct them.

5. Discussion and conclusions

This study investigated sources of error in medium-range (4–8 day) forecasts for Extratropical Cyclone Joachim, a unique case where medium-range forecasts predicted a large powerful cyclone would impact Europe, yet a less intense cyclone made landfall. A brief synoptic overview of the event revealed that the strength

of Joachim may have depended on its degree of phasing with a trough at the leading edge of a Rossby wave packet that originated over Alaska and traversed through a prominent northern stream over Canada to the western Atlantic Ocean. The ECMWF deterministic forecast initialized at 0000 UTC 11 December, which predicted Joachim would be intense, had a high degree of phasing between Joachim and this feature, while in reality, there was a lack of phasing between the northern and southern stream features. The synoptic analysis also revealed that the source of the Rossby wave packet associated with the development of Joachim was an intense ridge-building event over Alaska on 11 December 2011. To more thoroughly investigate the source of error in medium-range forecasts for this event, and in the process learn more about the origin and propagation of forecast errors in the midlatitudes, this study analyzed 5- and 6-day ECMWF ensemble forecasts for Cyclone Joachim. The origin of forecast errors is diagnosed by splitting the ensemble members into two subgroups, those that had a relatively accurate forecast of Joachim and those that forecasted Joachim would be quite intense, and then comparing the ensemble mean of the two subgroups against one another. The forecast differences were compared over several lead times to determine the dynamical processes responsible for an accurate forecast of Joachim versus a forecast for a strong Cyclone Joachim.

The primary distinctions between ensemble members that had a more accurate forecast of Joachim and those that did not were differences in synoptic waves moving poleward along the western side of an amplifying upper-tropospheric ridge (R2) south of Alaska on 11 December. Members with an accurate forecast of Joachim correctly predicted that this ridge would be more amplified and build farther poleward than what was forecast by members that predicted a strong Joachim. Statistical PV inversion of the PV differences between the two subgroups showed that a more amplified ridge acted as a more intense perturbation on the waveguide that had the effect of increasing the speed of a wave packet along the northern stream, leading to a lack of phasing between TN and a cyclone developing over the Gulf Stream on 14 December. In contrast, the slower eastward speed of the wave packet in the Strong members allowed TN to merge with the southern stream cyclone, leading to the development of a powerful cyclone. Relaxation experiments and forecast error calculations support the notion that the observed differences in the evolution of the northern streamflow in this forecast originate with differences in the location and strength of the ridge-building event (R2) over Alaska on 11 December.

The results of this study primarily agree with the established thinking of how errors in forecasts for the midlatitudes are structured and propagate. Forecast errors that lead to erroneous predictions of the strength of Joachim maximized on the tropopause and propagated downstream in wave-packet-like structures. This aligns well with the results of Szunyogh et al. (2000), Langland et al. (2002), and Hakim (2005).

Although only a case study, these results present further evidence that subsynoptic errors in the warm sector of a cyclone can be a significant source of error and uncertainty in forecasts for areas farther downstream. The ridge building that occurs in the warm sector of extratropical cyclones (WCB) can modulate the speed of subsynoptic features in the waveguide, which can significantly alter the weather downstream (e.g., Dirren et al. 2003; Davies and Didone 2013; Grams et al. 2011; Torn 2010). Moreover, there is reason to believe these areas may have larger analysis errors. One reason for this is that WCBs are often associated with extensive cloud cover, which limits the amount of satellite radiance data that is assimilated into operational models. This may have been especially problematic in medium-range forecasts of Joachim, as the WCB that caused uncertainties in these medium-range forecasts was located over the Pacific Ocean, where there are no ground or radiosonde observations to augment satellite radiance data. The results of this study suggest that medium-range forecasts of Joachim could have been improved by synoptic sampling of R2 (the warm sector of C2). More research is required to test this theory and further quantify the impact that uncertainty in WCBs has on the predictability of the downstream state.

Finally, this study also highlights the efficacy of diagnosing forecast errors by splitting ensemble forecasts into two subgroups and comparing the mean of the subgroups against one another. The clear and consistent results across different forecast initializations that result from this technique suggest that it is a robust and insightful method of diagnosing forecast errors. However, it is critical to have a large sample of forecasts and a reasonable forecast metric on which to split the ensemble.

Acknowledgments. The TIGGE data used in this study were retrieved from the NCAR (http://rda.ucar.edu/datasets/ds330.0/) and the ECMWF (http://apps.ecmwf.int/datasets/data/tigge/levtype=sfc/type=cf/) TIGGE data portals. We thank NCAR and ECMWF for the development of these user-friendly portals and for taking on the challenge of archiving such a large dataset. This research was supported by NOAA Award NA01NWS4680002, National Science Foundation Award 1461753, and the American Meteorological Society Graduate Fellowship Program.

REFERENCES

AIR Worldwide, 2011: Summary—Extratropical Cyclone Joachim. [Available online at http://alert.air-worldwide.com/EventSummary.aspx?e=596&tp=31&c=1.]

Blake, E., E. Rappaport, C. Landsea, N. Miami, and F. Miami, 2007: The deadliest, costliest, and most intense United States tropical cyclones from 1851 to 2006 (and other frequently requested hurricane facts). NOAA Tech. Memo. NWS TPC-5, 43 pp. [Available online at http://www.nhc.noaa.gov/pdf/NWS-TPC-5.pdf.]

Bougeault, P., and Coauthors, 2010: The THORPEX Interactive Grand Global Ensemble. *Bull. Amer. Meteor. Soc.*, **91**, 1059–1072, doi:10.1175/2010BAMS2853.1.

Buizza, R., J. R. Bidlot, N. Wedi, M. Fuentes, M. Hamrud, G. Holt, and F. Vitart, 2007: The new ECMWF VAREPS (Variable Resolution Ensemble Prediction System). *Quart. J. Roy. Meteor. Soc.*, **133**, 681–695, doi:10.1002/qj.75.

Chagnon, J. M., S. L. Gray, and J. Methven, 2013: Diabatic processes modifying potential vorticity in a North Atlantic cyclone. *Quart. J. Roy. Meteor. Soc.*, **139**, 1270–1282, doi:10.1002/qj.2037.

Chang, E. K. M., and I. Orlanski, 1993: On the dynamics of a storm track. *J. Atmos. Sci.*, **50**, 999–1015, doi:10.1175/1520-0469(1993)050<0999:OTDOAS>2.0.CO;2.

——, M. Zheng, and K. Raeder, 2013: Medium-range ensemble sensitivity analysis of two extreme pacific extratropical cyclones. *Mon. Wea. Rev.*, **141**, 211–231, doi:10.1175/MWR-D-11-00304.1.

Davies, H. C., and M. Didone, 2013: Diagnosis and dynamics of forecast error growth. *Mon. Wea. Rev.*, **141**, 2483–2501, doi:10.1175/MWR-D-12-00242.1.

Dirren, S., M. Didone, and H. C. Davies, 2003: Diagnosis of "forecast-analysis" differences of a weather prediction system. *Geophys. Res. Lett.*, **30**, 2060, doi:10.1029/2003GL017986.

Enz, R., P. Zimmerli, and S. Schwartz, 2009: Natural catastrophes and man-made disasters in 2008: North America and Asia suffer heavy losses. Sigma News Release, Swiss Reinsurance Company Ltd., Zurich, Switzerland, 41 pp.

Grams, C. M., and Coauthors, 2011: The key role of diabatic processes in modifying the upper-tropospheric wave guide: A North Atlantic case-study. *Quart. J. Roy. Meteor. Soc.*, **137**, 2174–2193, doi:10.1002/qj.891.

Hakim, G. J., 2003: Developing wave packets in the North Pacific storm track. *Mon. Wea. Rev.*, **131**, 2824–2837, doi:10.1175/1520-0493(2003)131<2824:DWPITN>2.0.CO;2.

——, 2005: Vertical structure of midlatitude analysis and forecast errors. *Mon. Wea. Rev.*, **133**, 567–578, doi:10.1175/MWR-2882.1.

——, and R. D. Torn, 2008: Ensemble synoptic analysis. *Synoptic–Dynamic Meteorology and Weather Analysis and Forecasting: A Tribute to Fred Sanders*, *Meteor. Monogr.*, No. 55, Amer. Meteor. Soc., 147–162, doi:10.1175/0065-9401-33.55.147.

——, D. Keyser, and L. F. Bosart, 1996: The Ohio Valley wave-merger cyclogenesis event of 25–26 January 1978. Part II: Diagnosis using quasigeostrophic potential vorticity inversion. *Mon. Wea. Rev.*, **124**, 2176–2205, doi:10.1175/1520-0493(1996)124<2176:TOVWMC>2.0.CO;2.

Hoskins, B. J., M. E. McIntyre, and A. W. Robertson, 1985: On the use and significance of isentropic potential vorticity maps. *Quart. J. Roy. Meteor. Soc.*, **111**, 877–946, doi:10.1002/qj.49711147002.

Joos, H., and H. Wernli, 2012: Influence of microphysical processes on the potential vorticity development in a warm conveyor belt: A case-study with the limited-area model COSMO. *Quart. J. Roy. Meteor. Soc.*, **138**, 407–418, doi:10.1002/qj.934.

Jung, T., M. J. Miller, and T. N. Palmer, 2010a: Diagnosing the origin of extended-range forecast errors. *Mon. Wea. Rev.*, **138**, 2434–2446, doi:10.1175/2010MWR3255.1.

——, T. N. Palmer, M. J. Rodwell, and S. Serrar, 2010b: Understanding the anomalously cold European winter of 2005/06 using relaxation experiments. *Mon. Wea. Rev.*, **138**, 3157–3174, doi:10.1175/2010MWR3258.1.

Langland, R. H., M. A. Shapiro, and R. Gelaro, 2002: Initial condition sensitivity and error growth in forecasts of the 25 January 2000 East Coast snowstorm. *Mon. Wea. Rev.*, **130**, 957–974, doi:10.1175/1520-0493(2002)130<0957:ICSAEG>2.0.CO;2.

Leutbecher, M., J. Barkmeijer, T. N. Palmer, and A. J. Thorpe, 2002: Potential improvement to forecasts of two severe storms using targeted observations. *Quart. J. Roy. Meteor. Soc.*, **128**, 1641–1670, doi:10.1002/qj.200212858313.

Livezey, R. E., and W. Y. Chen, 1983: Statistical field significance and its determination by Monte Carlo techniques. *Mon. Wea. Rev.*, **111**, 46–59, doi:10.1175/1520-0493(1983)111<0046:SFSAID>2.0.CO;2.

Majumdar, S. J., K. J. Sellwood, D. Hodyss, Z. Toth, and Y. Song, 2010: Characteristics of target areas selected by the ensemble transform Kalman filter for medium-range forecasts of high-impact winter weather. *Mon. Wea. Rev.*, **138**, 2803–2824, doi:10.1175/2010MWR3106.1.

Orlanski, I., and J. P. Sheldon, 1995: Stages in the energetics of baroclinic systems. *Tellus*, **47A**, 605–628, doi:10.1034/j.1600-0870.1995.00108.x.

Park, Y. Y., R. Buizza, and M. Leutbecher, 2008: TIGGE: Preliminary results on comparing and combining ensembles. *Quart. J. Roy. Meteor. Soc.*, **134**, 2029–2050, doi:10.1002/qj.334.

Richardson, D., J. Bidlot, L. Ferranti, T. Haiden, T. Hewson, M. Janousek, F. Prates, and F. Vitart, 2013: Evaluation of ECMWF forecasts, including 2012–2013 upgrades. ECMWF Tech. Memo. 710, ECMWF, Reading, United Kingdom, 53 pp. [Available online at http://www.ecmwf.int/sites/default/files/elibrary/2013/11921-evaluation-ecmwf-forecasts-including-2012-2013-upgrades.pdf.]

Riemer, M., and S. C. Jones, 2010: The downstream impact of tropical cyclones on a developing baroclinic wave in idealized scenarios of extratropical transition. *Quart. J. Roy. Meteor. Soc.*, **136**, 617–637, doi:10.1002/qj.605.

Schemm, S., H. Wernli, and L. Papritz, 2013: Warm conveyor belts in idealized moist baroclinic wave simulations. *J. Atmos. Sci.*, **70**, 627–652, doi:10.1175/JAS-D-12-0147.1.

Simmons, A. J., and B. J. Hoskins, 1979: The downstream and upstream development of unstable baroclinic waves. *J. Atmos. Sci.*, **36**, 1239–1254, doi:10.1175/1520-0469(1979)036<1239:TDAUDO>2.0.CO;2.

Swanson, K. L., and P. J. Roebber, 2008: The impact of analysis error on medium-range weather forecasts. *Mon. Wea. Rev.*, **136**, 3425–3431, doi:10.1175/2008MWR2475.1.

Szunyogh, I., Z. Toth, R. E. Morss, S. J. Majumdar, B. J. Etherton, and C. H. Bishop, 2000: The effect of targeted dropsonde observations during the 1999 Winter Storm Reconnaissance Program. *Mon. Wea. Rev.*, **128**, 3520–3537, doi:10.1175/1520-0493(2000)128<3520:TEOTDO>2.0.CO;2.

Torn, R. D., 2010: Diagnosis of the downstream ridging associated with extratropical transition using short-term ensemble forecasts. *J. Atmos. Sci.*, **67**, 817–833, doi:10.1175/2009JAS3093.1.

——, J. S. Whitaker, P. Pegion, T. M. Hamill, and G. J. Hakim, 2015: Diagnosis of the source of GFS medium-range track errors in Hurricane Sandy (2012). *Mon. Wea. Rev.*, **143**, 132–152, doi:10.1175/MWR-D-14-00086.1.

Tribbia, J. J., and D. P. Baumhefner, 2004: Scale interactions and atmospheric predictability: An updated perspective. *Mon. Wea. Rev.*, **132**, 703–713, doi:10.1175/1520-0493(2004)132<0703:SIAAPA>2.0.CO;2.

Wernli, H., 1997: A Lagrangian-based analysis of extratropical cyclones. II: A detailed case-study. *Quart. J. Roy. Meteor. Soc.*, **123**, 1677–1706, doi:10.1002/qj.49712354211.

Zhang, F., C. Snyder, and R. Rotunno, 2002: Mesoscale predictability of the surprise snowstorm of 24–25 January 2000. *Mon. Wea. Rev.*, **130**, 1617–1632, doi:10.1175/1520-0493(2002)130<1617:MPOTSS>2.0.CO;2.

Zheng, M., E. K. M. Chang, and B. A. Colle, 2013: Ensemble sensitivity tools for assessing extratropical cyclone intensity and track predictability. *Wea. Forecasting*, **28**, 1133–1156, doi:10.1175/WAF-D-12-00132.1.